Clim. Past Discuss., 6, 2117–2158, 2010
www.clim-past-discuss.net/6/2117/2010/
doi:10.5194/cpd-6-2117-2010


Climate of the Past Discussions



# Rapid shifts in South American montane climates driven by $p\mathrm{CO_2}$ and ice volume changes over the last two glacial cycles

**M. H. M. Groot[1], R. G. Bogotá[1,2], L. J. Lourens[3], H. Hooghiemstra[1], M. Vriend[1,†], J. C. Berrio[4], E. Tuenter[5], J. van der Plicht[6], B. van Geel[1], M. Ziegler[3], S. L. Weber[3], A. Betancourt[1], L. Contreras[1], S. Gaviria[7], C. Giraldo[1], N. González[1], J. H. F. Jansen[8], M. Konert[9], D. Ortega[1], O. Rangel[10], G. Sarmiento[7], J. Vandenberghe[9], T. van der Hammen[11], M. van der Linden[1], and W. Westerhoff[12]**

[1]University of Amsterdam, Institute for Biodiversity and Ecosystem Dynamics, Science Park 904, 1098 XH Amsterdam, The Netherlands
[2]Universidad Distrital, Facultad del Medio Ambiente y Recursos Naturales, Bogotá, Colombia
[3]University of Utrecht, Faculty of Geosciences, Utrecht, The Netherlands
[4]University of Leicester, Department of Geography, Leicester, UK
[5]University of Utrecht, Faculty of Science, Utrecht, The Netherlands
[6]University of Groningen, Centre for Isotope Research, Groningen, The Netherlands

[7]Universidad Nacional de Colombia, Facultad de Sciencias, Depto. de Geosciencias, Bogotá, Colombia
[8]Royal Netherlands Institute for Sea Research, Texel, The Netherlands
[9]Vrije Universiteit Amsterdam, Institute of Earth Sciences, Department of Paleoclimatology and Geomorphology, Amsterdam, The Netherlands
[10]Universidad Nacional de Colombia, Instituto de Ciencias Naturales, Bogotá, Colombia
[11]Fundacion Tropenbos, Bogotá, Colombia
[12]Deltares, Subsurface and Groundwater Systems, Geological Survey of the Netherlands, Utrecht, The Netherlands
[†]deceased

Received: 31 August 2010 – Accepted: 23 September 2010 – Published: 8 October 2010

Correspondence to: M. H. M. Groot (m.h.m.groot@uva.nl)

Published by Copernicus Publications on behalf of the European Geosciences Union.

## Abstract

Tropical montane biome migration patterns in the northern Andes are found to be coupled to glacial-induced mean annual temperature (MAT) changes; however, the accuracy and resolution of current records are insufficient to fully explore their magnitude and rates of change. Here we present a ~60-year resolution pollen record over the past 284 000 years from Lake Fúquene (5° N) in Colombia. This record shows rapid and extreme MAT changes at 2540 m elevation of up to 10 ± 2 °C within a few hundred of years that concur with the ~100 and 41-kyr (obliquity) paced glacial cycles and North Atlantic abrupt climatic events as documented in ice cores and marine sediments. Using transient climate modelling experiments we demonstrate that insolation-controlled ice volume and greenhouse gasses are the major forcing agents causing the orbital MAT changes, but that the model simulations significantly underestimate changes in lapse rates and local hydrology and vegetation feedbacks within the studied region due to its low spatial resolution.

## 1 Introduction

Long and high-resolution records of climate change are mainly inferred from ice cores of Greenland and Antarctica (GRIP-Members, 1993; Grootes et al., 1993; Jouzel et al., 2007; NGRIP-Members, 2004; Parrenin et al., 2007; Svensson et al., 2008), marine sediments (Bond et al., 1993; Martrat et al., 2007; Peterson et al., 2000), and speleothems (Cheng et al., 2009; Wang et al., 2008). High altitude regions in the tropics on the other hand appear to be particularly sensitive to current climate changes (Urrutia and Vuille, 2009) and are therefore ideally suited to investigate the environmental response (i.e. glaciations, hydrology and ecosystem integrity) to $p\mathrm{CO_2}$ and glacial-induced ice volume variations rather than their surrounding lowlands. These high altitude tropical settings lack, however, the necessary high-resolution and accurate records to fully explore the operating mechanisms of the Earth's climate system.

Here we elaborate on previous investigations (Hooghiemstra, 1984; Mommersteeg, 1998; Torres et al., 2005; Van der Hammen, 1974; Van der Hammen and González, 1960; van Geel and van der Hammen, 1973; Wille et al., 2001) by establishing an ultra-high resolution (i.e. ~60 year between 4646 time slices) pollen-based record of climate change from Lake Fúquene in the Eastern Cordillera of Colombia (5°28′ N, 73°45′ W, 2540 m), which may compete in accuracy with the data collected from the ice cores, speleothems and marine sediments.

The modern precipitation regime at Lake Fúquene (Fig. 1) is controlled by the annual migration of the inter tropical convergence zone (ITCZ) causing two dry seasons (December to February and from June to August) and two rainy seasons (March to May and from September to November). The seasonal temperature cycle is very weak with monthly temperatures of 13° to 14 °C. The daily temperature range is large and during the dry season night frost may occur (van Geel and van der Hammen, 1973). At present the lake lies within the Andean forest belt (Fig. 2). The upper boundary of this belt or upper forest line (UFL) coincides approximately with the 9.5 °C mean annual isotherm, while the lower boundary is at an elevation where night frost no longer occurs (Hooghiemstra, 1984; Van der Hammen, 1974; Van der Hammen and González, 1960). During glacial conditions, lower temperatures cause a descend in altitudinal position of individual taxa, leading to a lowering of main vegetation belts (Hooghiemstra, 1984; Van't Veer and Hooghiemstra, 2000; Van't Veer et al., 1995; Van der Hammen, 1974; Van der Hammen and González, 1960; Wille et al., 2001). We will use the changes in percentages of arboreal pollen (AP%) (Hooghiemstra, 1984; Van der Hammen and González, 1960) to resolve the orbital and sub-Milankovitch mean annual temperature variations at Lake Fúquene over the past 284 000 years. In addition, we have carried out three transient climate modelling experiments to explore the significance of orbitally induced insolation, $p\mathrm{CO}_2$ and glacial-induced ice albedo feedback mechanisms on the reconstructed temperature variations.





CPD
6, 2117–2158, 2010

## 2 Material and methods

### 2.1 Sediment cores

Two ∼60 m long sediment cores, Fúquene-9 (Fq-9) and Fúquene-10 (Fq-10) were retrieved from Lake Fúquene, using a floating platform with Longyear drilling equipment of Gavesa Drilling Co. Bogotá. Consolidated sediments were first approached at c. 6 m below the water surface. Sediments were retrieved in segments of 100 cm length with a diameter of 75 mm. Core samples at the two drilling sites were collected with 50 cm overlapping depth intervals to maximize sediment recovery (Table 1). Undisturbed sediments in pvc-tubes were directly transported by air freight to The Netherlands for further treatment. The fresh sediment surface was photographed in a standardized photographic room. The two cores were transported to the NIOZ laboratory (Texel, The Netherlands) to obtain along the full length of both cores XRF-based geochemical data. Subsequently the cores were transported to the University of Amsterdam for collecting > 5000 samples for pollen and grain size analysis. Grain size analysis was carried out at the Vrije Universiteit Amsterdam.

### 2.2 Analytical methods

Bulk chemistry was measured with an Avaatech X-ray fluorescence (XRF) core scanner at the Royal Netherlands Institute for Sea Research (NIOZ). The XRF core cortex-scanner counts the number of the chemical elements aluminum (Al, atomic number 13) to bismuth (Bi, atomic number 83) per second (cps) directly at the surface of a split sediment core, a measurement which is proportional to chemical concentrations (Jansen et al., 1998). Prior to the measurement, the split core surface was smoothed horizontally without contaminating sediment surface. Subsequently the surface was covered with a 4 µm thin SPEXCerti Prep Ultralene foil to avoid contamination of the X-ray unit during measurement and to avoid desiccation of the sediment. Air bubbles under the foil were carefully removed. Measurements were carried out at 1 cm increments along





CPD
6, 2117–2158, 2010

the full length of the 60 m long cores. We used generator settings of 10 kV and 30 kV and measurement time was 30 s per cm. The standard procedure included a control measurement with a standard after every 1 m core interval. Further technical and practical details about the XRF core scanner are described in Richter et al. (2006).

### 2.3 Pollen analysis

The Fq-9C record was examined at 1 cm increments for a detailed survey of the palynological content. Pollen samples of 1 $cm^3$ were processed using the standard pretreatment including sodium pyrophosphate, acetolysis, and heavy liquid (bromoform) separation. We counted pollen and spore taxa with specific ecological envelopes and a clear response to climate change through altitudinal shifts (Hooghiemstra, 1984; Mommersteeg, 1998; Torres et al., 2005; Van't Veer and Hooghiemstra, 2000; Van der Hammen and González, 1960; Wille et al., 2001). Pollen types were assigned to the following ecological groups: (1) taxa of subandean forest, (2) taxa of Andean forest, (3) taxa of subpáramo vegetation, (4) taxa of grasspáramo vegetation and (5) taxa indicating dry conditions. Down core changes in the relative contribution of the pollen types in these ecological groups reflect altitudinal shifts of the main ecological groups. Following Van der Hammen and González (1960) and Hooghiemstra (1984) AP% were used to estimate the position of UFL along the record.

## 3 Results

### 3.1 Composite section

Cores Fq-9 and Fq-10 were used to build a composite record (Fq-9C) with a minimal number of gaps in the sedimentary sequence. Down core changes in the lithology represent the first information for this exercise. Distinct and repetitive layers with peat, and intervals with higher concentrations of aeolian dispersed fine grained volcanic ash



Discussion Paper | Discussion Paper | Discussion Paper | Discussion Paper |

CPD

6, 2117–2158, 2010

Rapid shifts in South American montane climates over the past 284 000 years

M. H. M. Groot et al.

allowed an adequate first correlation between cores. Subsequently, we used records of Fe and Zr obtained by X-ray fluorescence at 1 cm distance over the full length of both cores to fine tune the correlation. Selection of iron (Fe) and zircon (Zr) out of the suite of measured elements is justified by their physical and chemical properties. During XRF measurements heavier elements (Fe and Zr) remain relatively unaffected by the variation of physical properties along the core. In addition, Fe and Zr content may be indicative of variations in source areas and/or variations in sedimentary environments. It is to be expected that changes in both variables coincide simultaneously within the two parallel cores. For instance, Fe supply to the Fúquene basin may be associated with airborne volcanic ash. Ash layers have a distinct yellow color due to neo-formed siderite ($FeCO_3$) (Sarmiento et al., 2008). The Fe content may also be influenced by changes in the redox state of the water column as well as the sediment columns (Davidson, 1993). The latter may be associated with lake level changes which cause alternations between submersed lacustrine environments to shallow swampy conditions, and even to a drained status of the lake. Zircon is a conservative element and relatively resistant to chemical weathering processes (Balan et al., 2001). Zircon is found as detrital grains in igneous, metamorphic, and sedimentary rocks. The zircon content is positively correlated with weight percent of coarse silt plus sand (Alfonso et al., 2006; Nyakairu and Koeberl, 2002; Stiles et al., 2003). Therefore, Zr may reflect high energetic sedimentary environments mostly coinciding with a proximal sediment source in relation to the drilling location of the cores.

Core Fq-9 had the least technical drilling artifacts and was therefore used as the backbone for our study. This implies that the depth of Fq-10 was adjusted so that the patterns of the various proxy records from both cores aligned. The procedure was carried out as follows: (1) High resolution photographs of the freshly split sediment cores and binocular-based lithological descriptions (Sarmiento et al., 2008) were used to obtain an initial framework of stratigraphic correlation. (2) Time series of Fe and Zr content of Fq-9 and Fq-10 were visually matched using Analyseries 1.2 software (Paillard et al., 1996). Tie points were preferably chosen at the steepest parts of the





CPD
6, 2117–2158, 2010

curves; occasionally maxima or minima were used (Table 2). The matched records were compared with the initial stratigraphic framework. (3) The procedure described in points (1) and (2) was repeated until all paired proxy records, e.g. Fe, showed comparable variation at any given depth. (4) No adjustments, such as squeezing and stretching were introduced within core segments. All core segments of Fq-10 were depth-shifted and stratigraphically aligned relative to the Fq-9 core segments. Subsequently, a final composite core was built where inclusion of disturbed intervals and sediment gaps was minimized (Table 3).

The composite core was labeled as Fq-9C and represents 90% of the sediment infill of the uppermost 60 m of the Fúquene Basin. Average lateral offset between stratigraphic layers was 52 cm (Fig. 3). Offsets between cores may reflect difference in sedimentation rates, erosion, and methane emissions during the drilling procedure. Sediments between 26 and 21 m contain significant proportions of organic matter. Interval 22 to 20.8 m reflects compressed peat. This 5 m of sediments contained over pressured methane which escaped from the borehole when the corer contacted this reservoir at 21 m depth. For safety reasons drilling activities were laid down during a full day until sediments dissipated (GAVESA, 2002). The escape of methane and subsequent compaction of the peat explains the significant change in offset between both cores in this core interval (Fig. 3). The lake surface was used as a reference. During the 5 weeks long drilling operation, lake-level changes were noticed after periods of heavy rains. As a consequence the offset between the zero calibration points of cores Fq-9 and Fq-10 is estimated offset up to 20 cm.

### 3.2 Spectral analysis

The AP% of Fq-9C fluctuates between 2% and 98% with the highest values found between 21 and 26 mcd and the lowest around 10, 29 and 53 mcd (Fig. 4a). We submitted the AP% record to spectral analysis in the depth domain using the CLEAN algorithm (Roberts et al., 1987), the REDFIT program (Schulz and Mudelsee, 2002)





CPD
6, 2117–2158, 2010

and a Blackman-Tukey power spectrum (Blackman and Tuckey, 1958) to identify the possible imprint of orbital signals.

The CLEAN algorithm was run as a MATLAB routine (Heslop and Dekkers, 2002) and is particular robust in determine the frequency distribution of unevenly spaced data series and noisy signals (Baisch and Bokelmann, 1999; Roberts et al., 1987). The CLEAN procedure performs a nonlinear deconvolution in the frequency domain in order to remove any artifacts resulting from incomplete sampling in the time (depth) domain. It includes a series of Monte Carlo simulations which allow a large number of slightly different spectra to be generated for a single input signal. The differences between these spectra are utilized to determine a mean spectrum and confidence intervals both for individual frequency peaks and for the spectrum as a whole. Through the use of an Inverse Fourier Transform of the MC-CLEAN spectrum, the data can be reconstructed in the time domain, providing a "noise free" version of the input signal. Because of the large number of data points and the almost equally spaced sampling resolution, we choose to linearly detrend the AP% depth series and slightly smooth it with a 5 cm average to reduce the number of data points from 4868 to 1134 before the CLEAN analysis (Fig. 4b). The CLEAN spectrum was subsequently determined by adding 10% red noise (i.e. control parameter = 0.1), a clean/gain factor of 0.1, 500 CLEAN iterations, an interpolation step (dt) value of 5 cm and 500 simulation iterations (Fig. 5a). The resulting spectrum revealed highly significant (99%) peaks at 9.07 and 22.65 m, and less significant peaks at 12.58, 5.96, 4.19 and 3.65 m. The 22.65 m periodicity coincides with the large-scale changes in the AP% record, which we attribute to the imprint of the late Pleistocene ~100 kyr glacial rhythm (Hooghiemstra et al., 1993). Accordingly, the 9.07 m cycle corresponds with a 41-kyr period, indicating a large obliquity control of the climate variability in this region.

We evaluated the CLEAN spectral outcome first by comparison with a Blackman-Tukey power spectrum, which was performed with AnalySeries 2.2 (Paillard et al., 1996) using 75% of the 200-year interpolated time series, a Parzen window and a Band Width of 0.0087. Although the power spectrum is much more smoothed, strong peaks





CPD
6, 2117–2158, 2010

occur at ∼9 and 25 m; consistent with the CLEAN estimates (Fig. 5b). Secondly, we applied the computational spectral analysis program, REDFIT version 3.8 (Schulz and Mudelsee, 2002) on the original (non-smoothed and non-detrended) AP% data set. In this model a first-order autoregressive progress (AR1), which is assumed to present a good estimate of the red-noise signature, is estimated directly from the (unevenly spaced) time series and, subsequently, transferred into the frequency domain using the Lomb-Scargel algorithm. Confidence levels based on a $\chi^2$ distribution are calculated from the AR1-noise and from percentiles of the Monte Carlo ensemble. For the analysis, we applied one Welch Overlapped Segment Averaging (WOSA) segment ($n_{50} = 1$), 2000 Monte Carlo simulations ($N_{sim} = 2000$), and a rectangular window ($I_{win} = 0$). This resulted in a value of $\tau$ of 20.9 with 2 degrees of freedom. The power estimate and distribution are in good agreement with that of the Blackman-Tukey method, although an additional peak is found at 1193 cm (Fig. 5b and d). Third, we have run the CLEAN algorithm again, but in this case, D. Heslop (personal communication, 2009) incorporated the method of Mudelsee to estimate the AR1 characteristic period of the input data series (Mudelsee, 2002). With each iteration step, a new time series is calculated with the same AR1 characteristics and processed with CLEAN. These spectra are then used to calculate the confidence levels. This approach is a little different from before, because the noise is not added to the signal, but studied separately. This implies that the spectrum for the input data does not have error bounds, because it remains the same for each iteration step. Only the separate noise component is changing. The results are plotted in Fig. 5c and largely confirm the significance of the spectral peaks obtained from REDFIT.

### 3.3 Orbital tuning

We extracted the distinct 9 m component of the AP% record using a Gaussian filter as implemented in the freeware AnalySeries 2.2 (Paillard et al., 1996). The filtered frequency was centered at 0.0011 ± 0.0004 (Fig. 4b). The filtered 9 m signal was subsequently correlated to the filtered obliquity-related 41-kyr component of the LR04 benthic $\delta^{18}O$ record (Lisiecki and Raymo, 2005) to establish an age model for Fq-9C (Fig. 4c). For this purpose we applied a Gaussian filter centered at a frequency of $0.0245 \pm 0.002$, and tuned our data by peak-to-low matching of the filtered 9-m signal of core Fq-9C and the filtered 41-kyr signal in the LR04 record. Extrapolation of the resulting age model provides an age estimate for the bottom and top of the Fq-9C sedimentary sequence of respectively 284 and 27 kyr before present (ka), and an average sample resolution of ~60 yr.

Data from the last 27 kyr of the Fq-2 core (van Geel and van der Hammen, 1973) was implemented to construct a complete AP% record for the past 284 000 years. Correlations were verified through biostratigraphic events and radiometric carbon dates of the Fq-7C core (Hessler et al., 2009; Mommersteeg, 1998). For this purpose we revised the $^{14}C$ ages for the Fq-2 and Fq-7C records (Table 4) using the CALIB REV 5.0.2. program (Stuiver et al., 2009). Tie points between Fq-2, Fq-7C and Fq-9C were based on the following biostratigraphic markers: Arboreal Pollen, *Alnus*, *Polylepis-Acaena*, *Quercus*, *Myrica*, *Podocarpus*, *Asteraceae tubuliflorae*, *Hypericum* (Table 4). Detail comparison between record Fq-2 and Fq-7C for the upper part of the record showed that the Younger Dryas is only present in core Fq-2. Therefore, we linked Fq-9C directly to Fq-2 at 27.19 ka to produce the Fúquene Basin Composite record (FqBC), which reach up to the latest Holocene (Fig. 6).

Correlation to the LR04 $\delta^{18}O_{benthic}$ record was chosen, because this record is used as the backbone for many late Pleistocene paleoclimate studies. The LR04 chronology follows the SPECMAP approach (Imbrie et al., 1984; Imbrie and Imbrie, 1980) in which the $\delta^{18}O_{benthic}$ record is tuned to a simple ice sheet model that includes a forcing function (i.e. 21 June insolation curve for 65° N), an average ice-sheet response time and a non-linearity coefficient that describes the slow build-up and fast terminations of the ice-sheets. For the past 300 000 years, the LR04 chronology yields time lags for the obliquity (41-kyr) and precession (23-kyr) components of the $\delta^{18}O_{benthic}$ record of $7.5 \pm 0.8$ and $4.5 \pm 0.5$ kyr, respectively. This implies that also the AP% time series includes a ~7.5 kyr time lag for its obliquity-related component, which is supported





CPD
6, 2117–2158, 2010

by the compliance between the tuned ages of positions 300 and 353 cm in Fq-9C of respectively 32.9 and 35.2 ka, and their corresponding corrected radiocarbon ages of 32.54 ± 0.32 and 35.74 ± 0.31 (Fig. 6).

## 4 Discussion

### 4.1 Mean annual temperature reconstructions

Our new record radically improved the temporal resolution of the earlier pollen based records from the Fúquene Basin with an order of magnitude. The new pollen record covers the last two glacial cycles with better than centennial resolution. Evidently, the FqBC depicts the last three glacial terminations, $T_I - T_{II}$, $T_{\mathrm{IIIa}}$ and $T_{\mathrm{IIIb}}$ (Fig. 6). Wavelet analysis reveals highly significant spectral power at the glacial-bound 41 and 113-kyr periods, a continuum power distribution in the range of 9–13, 16–19 and 25–32 kyr, and enhanced power in the ~8 kyr frequency band at the major terminations (Fig. 7).

From previous altitudinal pollen studies of the tropical Andes, it appeared that changes in AP% respond quasi-linearly to temperature-driven vertical shifts in the UFL between 3700 m (the highest mountains at close distance) and the LGM position at ~2000 m (Hooghiemstra, 1984; Hooghiemstra and Van der Hammen, 1993; Van't Veer and Hooghiemstra, 2000; Van der Hammen, 1974; Van der Hammen and González, 1960; Wille et al., 2001). During the LGM, MAT at Lake Fúquene was approximately 7.8 °C lower than at present (Hooghiemstra, 1984; Hooghiemstra et al., 1993; Van't Veer and Hooghiemstra, 2000; Van der Hammen, 1974; Van der Hammen and González, 1960; Wille et al., 2001). This pollen based estimate is in good agreement with the 5–9 °C decrease derived from the change in snowline along the Eastern Cordilleras of the central Andes (Klein et al., 1999). In addition, these pollen studies showed that the LGM lapse rate was much steeper (~0.76 °C/100 m) (Wille et al., 2001) than today (0.6–0.64 °C/100 m) (Florez, 1986). The resulting 3 to 5 °C LGM decrease in sea surface temperatures (SST) is consistent with the ~3 ± 1 °C lowering derived from





CPD
6, 2117–2158, 2010

the Mg/Ca and $U^{k'}_{37}$ – based temperature reconstructions of cores TR163-19 (Lea et al., 2000) and MD02-2529 (Leduc et al., 2007) in the Equatorial Pacific (Figs. 1 and 6).

Hence, we may use the AP% to provide a good approximation of MAT at Lake Fúquene through time using the modern to glacial temperature difference. However, since the AP% record is biased by the destruction of montane forests through intensive agriculture and soil erosion in the area over the last 3000 years (van Geel and van der Hammen, 1973), we assigned the AP% of 73 ± 6% at ~3.1 ka a MAT of 13.5 °C, assuming that MAT remained close to present-day values over the past 3 ka (van Geel and van der Hammen, 1973). With a mean AP% value of 15 ± 6% at ~20 ka, this implies that a change in AP% of 10% corresponds with a MAT change of 1.3 ± 0.3 °C. The estimated standard error of the presented MAT record (Fig. 6) is 0.6 ± 0.4 °C, considering a mean temperature difference between 20 and 3 ka of 7.8 °C (Hooghiemstra, 1984; Hooghiemstra et al., 1993; Van't Veer and Hooghiemstra, 2000; Van der Hammen, 1974; Van der Hammen and González, 1960; Wille et al., 2001). The resulting MAT estimate of 15 ± 1.5 °C at 7 ka (early Holocene) is consistent with earlier reconstructions (van Geel and van der Hammen, 1973).

Comparison between our reconstructed MAT at Lake Fúquene and the Mg/Ca-derived SST estimates of core TR163-19 for the last 284 000 years shows that the temperature variations at high altitudes in the tropical northern Andes are larger and much more rapid, i.e. up to 10 ± 2 °C within a few hundred of years, than reflected in the equatorial marine record (Fig. 6). They are slightly smaller in amplitude, although within error, than the reconstructed continental mean annual air temperature ($T_{air}$) variations between 40 and 80° N (Bintanja et al., 2005) and Antarctic temperatures (Jouzel et al., 2007; Parrenin et al., 2007) (Fig. 6). We obtained a considerable longer duration for MIS 5.5 (defined by the temperatures above present-day values between 110–133 ka) than the marine and polar temperature records (120–132 ka). A longer duration for MIS 5.5 is, however, in good agreement with the radiometric dated sea level records (Blanchon et al., 2009; Gallup et al., 2002; Thompson and Goldstein, 2006) during this period (Fig. 7).

### 4.2 Comparison with transient climate modelling experiments

We have performed three transient climate modelling experiments with a GCM of intermediate complexity, CLIMBER-2.3 (Petoukhov et al., 2000), over the past 284 ka to serve an explanation for the MAT record in terms of regional versus globally-induced temperature variations. For this purpose we used a coupled model of intermediate complexity, CLIMBER-2 (version 3) (Petoukhov et al., 2000), that is very suitable for long transient simulations due to its fast turnaround time (Calov et al., 2005a, b; Claussen et al., 1999; Tuenter et al., 2005). The model consists of an atmosphere model, an ocean/sea-ice model and a land/vegetation model. No flux adjustments are used. The atmospheric model is a 2.5-dimensional statistical-dynamical model with a resolution of 10° in latitude and approximately 51° in longitude. The model does not resolve synoptic timescales but uses statistical characteristics associated with ensemble-means of the system. The vertical resolution for the circulation, temperature and humidity is 10 levels and for the radiation 16 levels. The time step is one day. The terrestrial vegetation model is VECODE (VEgetation COntinuous Description) (Brovkin et al., 1997). The model computes the fraction of the potential vegetation (i.e., grass, trees and bare soil). This is a continuous function of the annual sum of positive day-temperatures and the annual precipitation. The computed vegetation changes affect the land-surface albedo and the hydrological cycle. The time step of VECODE is one year. The ocean model (Stocker et al., 1992) describes the zonally averaged temperature, salinity and velocity for three separate basins (Atlantic, Indian and Pacific oceans). The three basins are connected by the Southern Ocean through which mass, heat and salt are exchanged. The latitudinal resolution is 2.5° and the vertical resolution is 20 unequal levels. The time step is 5 days. The ocean model includes a simple thermodynamic sea-ice model that computes the sea-ice fraction and thickness for each grid box, with a simple treatment of advection and diffusion of sea-ice. Results of CLIMBER-2 compare favorably with data of the present day climate (Ganopolski et al., 1998; Petoukhov et al., 2000) as do the results derived from sensitivity experiments





CPD
6, 2117–2158, 2010

(like changes in vegetation cover and solar irradiance) with those of more comprehensive models (Ganopolski and Rahmstorf, 2001).

Three transient simulations were carried out for the interval from 650 ka to present. Only the results for last 284 ka are discussed here (Fig. 7). The only forcing used in the EXP O simulation is insolation changes induced by the $La04_{(1,1)}$ orbital parameters, while the ice sheets volume and $CO_2$ forcing were kept fixed at present-day and pre-industrial (280 ppmv) values, respectively. In the EXP OI simulation the same orbital forcing was used but now varying ice-sheets on the Northern Hemisphere while in EXP OIG varying ice-sheets were included as well reconstructed changes in atmospheric greenhouse gas concentrations.

The greenhouse gas concentrations had to be prescribed because CLIMBER-2 does not contain a carbon cycle model. The used concentrations of $CO_2$ and $CH_4$ (methane) were mainly obtained from Antarctica ice cores together with other sources for the recent years. The measurements for 284 ka until the Holocene were taken from Vostok (Petit et al., 1999). For the Holocene, measurements from EPICA Dome C (Flückinger et al., 2002) were used because the sampling frequency is higher than for Vostok. Finally, for the last 500 years we used values from several sources (Robertson et al., 2001). The sampling frequencies for both $CO_2$ and $CH_4$ are irregular in time and are not similar for both gases. We interpolated both records to obtain annual values using cubic spline interpolation. Because CLIMBER-2 only has a $CO_2$-module and no $CH_4$-module, we had to transfer the $CH_4$ record into an equivalent $CO_2$ record assuming that $CH_4$ is 21 times as effective in absorbing long wave radiation than $CO_2$ (Lashof, 2000).

In addition, our version of CLIMBER-2 does not include an interactive ice-sheet model, so we had to prescribe the ice fraction and height of the Eurasian and North American ice sheet, which are considered to portray the largest ice sheet fluctuations during the studied time interval. The volumes for the Eurasian and North American ice sheets were obtained from a simulation with a 3-D ice sheet model (Bintanja et al., 2005) and translated into ice areas and heights of the ice sheets. For the ice areas the ICE-5G ice distribution of the LGM (21 ka) was used as reference (Peltier, 2004) and set on the spatial grid of CLIMBER-2 (Table 5). Due to a lowered sea level during the LGM and earlier glacial periods, ice was present on the increased land areas north of 60° N. Since the standard representation of the Earth's present-day geography in CLIMBER-2 does not take these larger land areas into account, we have increased the size of the land fractions from the northern Eurasian grid boxes for experiments OI and OIG. A test simulation using the extended land fraction but with present-day ice-sheet distribution was compared to a standard control run to examine possible climatic changes due to the modified land-sea distribution. Over the modified grid boxes the climate changed, but not significantly over the other grid boxes.

From the simulated volumes the time-varying heights of the American and the Eurasian ice-sheet was computed as follows: First, we let the Eurasian and American Ice-sheet have heights $H_{eur}$ and $H_{am}$ at some central grid boxes while at the surrounding grid boxes heights are $0.5\times H_{eur}$ and $0.5\times H_{am}$, respectively (Table 5). The volumes are estimated by multiplying the ice-covered area of an ice-covered grid box and the height of the ice-sheet in that grid box, adding the results for all ice-covered grid boxes. As the volumes are given from the 3-dimensional ice sheet model, $H_{eur}$ and $H_{am}$ can be computed. A drawback of this method is that only the height of the ice sheets change in time while the areas of the ice-sheets are fixed. Variations in height affect changes the atmospheric circulation, which results in climate variations especially above and to the East (i.e., downstream) of the ice-sheets. For the Fúquene area it is most likely that variations in albedo due to variations in ice-sheet area are more important than variations in height, because albedo variations directly affect the climate response to insolation variations. In order to let the area vary during the simulations, we instantly lowered the ice-fraction by 0.25 if $H_{eur}$ or $H_{am}$ becomes less than 1000 m and again by 0.25 for heights lower than 500, 100 and 10 m.

During the (prescribed) waxing and waning of the ice sheets there is no transport of water from the oceans to the ice sheets and vice versa, i.e., the sea-level in the model does not change during glacial cycles. For all simulations the height and surface area



Discussion Paper | Discussion Paper | Discussion Paper | Discussion Paper |

CPD

6, 2117–2158, 2010

Rapid shifts in South American montane climates over the past 284 000 years

M. H. M. Groot et al.

of Greenland and Antarctica as well as small glaciers were kept at present-day values. All three simulations have been carried out with the coupled atmosphere-ocean-vegetation model. The influence of interactive vegetation on the transient behavior of climate is described elsewhere (Tuenter et al., 2005). The initial states were obtained by performing a 5 kyr equilibrium run using the boundary conditions for 650 ka. The results are shown as averages over 100 yr as the periods of the oscillations of the orbital forcing and variations in ice-sheet volume and greenhouse gas concentration are much longer than 100 yr.

EXP O revealed only small temperature differences of less than ~0.8 °C, which oscillate primarily on a precession frequency (Fig. 7). A direct influence of orbital-induced insolation changes can therefore not explain the reconstructed large MAT shifts, which is in line with the absence of a distinct precession-related signal in the AP% record of Lake Fúquene. EXP OI clearly illustrates that ice volume changes largely control the MAT at ~2.5 km altitude in the tropical Andes, but alone they are insufficient to explain the whole magnitude of the MAT changes at Lake Fúquene (Fig. 7). Evidently, the modelled MAT compares much better with our data when greenhouse gas forcing (EXP OIG) is added. This supports recent modelling studies (Urrutia and Vuille, 2009), which project large changes in South American (sub)alpine climates by the end of the 21st century due to enhanced anthropogenic greenhouse gas emissions. However, the simulated glacial-interglacial MAT changes of 3 to 4 °C still significantly underestimate the reconstructed variations at Lake Fúquene (Fig. 7). Part of this discrepancy can be explained by the large divergence between simulated glacial-interglacial changes in lapse rate of less than 0.005 °C/100 m, and the reconstructed change in lapse rate of up to ~0.3 °C/100 m. Another important factor in controlling this offset is the low spatial resolution of CLIMBER, which excludes to resolve specific changes in the local hydrology and vegetation feedbacks within the studied region. Finally, our CLIMBER-2 runs strongly underestimate the sub-Milankovitch and millennial scale variability (i.e. < 11 kyr), which clearly affected the MAT at the lake.





CPD
6, 2117–2158, 2010

### 4.3 Correlation between land and ice records of climate change

The sub-Milankovitch MAT variability at Lake Fúquene appears one-to-one coupled to the millennial scale changes reflected in the Antarctica (deuterium) and Greenland ($\delta^{18}$O) temperature records (Fig. 8). In particular, the signature of the Younger Dryas, constrained by $^{14}$C dates, and the interstadial Dansgaard-Oeschger (DO) cycles 1 (Bølling-Allerød), 8, 12, 14, 19 and 20 suggest an unprecedented North Atlantic-equatorial link. In addition, the short interval with low MAT during MIS 5.5 and the rapid MAT changes during the penultimate glacial period and Termination II mirrors the Greenland Ice Core Project (GRIP) $\delta^{18}$O record (GRIP-Members, 1993). However, the lower part of the GRIP core is suspect to disturbance, since it shows a different pattern than the one found in the North Greenland Ice Core Project (NGRIP) (Svensson et al., 2008; NGRIP Members, 2004) and the nearby Greenland Ice Sheet Program 2 (GISP2) (Grootes et al., 1993), although gas measurements suggest that it contains ice of the last interglacial and penultimate glacial maximum (Landais et al., 2003). The North Greenland Eemian Ice Core Drilling Project (NEEM) may decipher the robustness of this correlation.

At present, we consider that the age constraints of our MAT record are not accurate enough to determine the exact phase relationship with the North Atlantic cold events: i.e. the warm events appear also closely linked to the inferred Antarctic Isotope Maximum (AIM) (Members, 2006) (Fig. 8). It is tempting, however, to link maximum MAT conditions at Lake Fúquene to interstadial periods, because palynological investigations of the Cariaco Basin off northern Venezuela (Fig. 1) revealed the highest pollen concentrations and the maximum extend of semi-deciduous and evergreen forests in the northernmost part of South America occurred during these times (González et al., 2008). During stadials, the region around the Cariaco Basin is characterized by increases of salt marshes, herbs, and montane forests, while during Heinrich (H) events, periods of massive ice rafting in the North Atlantic (Broecker, 1994), forest abundance decreased (González et al., 2008). It has been proposed that during these events, a





CPD
6, 2117–2158, 2010

reduced Atlantic meridional overturning circulation resulted in extreme winter cooling of the North Atlantic (Cheng et al., 2006; Denton et al., 2005). Through an atmospheric connection, the ITCZ was, probably also with a winter bias (Ziegler et al., 2008), shifted to a more southern position (Cane and Clement, 1999; Chiang et al., 2003; Clement and Peterson, 2008; Peterson et al., 2000), and causing wetter climate conditions in the north-eastern part of Brazil and the Bolivian Altiplano (Baker et al., 2001; Wang et al., 2004). A comparison with a detailed record of North Atlantic, $C_{37:4}$ alkenone record of the Iberian Margin (Martrat et al., 2007), shows that in particular during H1-2 and H6 Lake Fúquene was affected by the lowest MAT (Fig. 8).

## 5 Conclusions

A strong one-to-one coupling between tropical and the North Atlantic climate variability on orbital and millennial time scales is found based on a new ultra-high resolution pollen record from the Fúquene Basin in the northern Andes. Using climate modeling experiments, we have shown that the large-scale, orbital-induced vegetation changes can be explained by the ~100 kyr and obliquity (41 kyr) dominated glacial-interglacial global temperature variations and changes in greenhouse gas forcing. Besides, our study has revealed that (sub)alpine climates in the northern Andes and associated ecosystems react very sensitive (rapid) on global climate change, thereby supporting modelling studies of future climate change (Urrutia and Vuille, 2009).

*Acknowledgements.* We thank Gavesa Co. (Bogotá) for the dedicated drilling of the cores; B. Chaparro of the Corporacion Autónoma Regional (CAR) for permissions to work in Lake Fúquene; Tropenbos-Colombia (Carlos Rodriguez) for logistic support; Annemarie Philip for preparing pollen samples. Pollen analysis of the Fúquene-9C core was carried out by a team of trained palynologists consisting of Mirella Groot, Giovanni Bogotá, Juan Carlos Berrio, Alejandra Betancourt, Catalina Giraldo, Natalia González, Lineth Contreras, Diana Ortega, and Yahir Valderrama. The Fúquene Project is financially supported by NWO-ALW (J. C. B., L. J. L., and E. T.), WOTRO (J. C. B.), IBED (M. H. M. G.), and ALBan (R. G. B.). This paper is dedicated to the memory of Mirjam Vriend, who died in an accident.

H. H. and J. C. B. initiated and coordinated the project. M. H. M. G. and R. G. B. carried out most of the laboratory analyses and pollen diagrams. B. v. G. produced the Fq2 pollen record. M. V. produced the correlation between Fq9 and Fq10. Age model reconstruction and statistics were performed by L. J. L. Climate modelling experiments were designed by E. T. and S. L. W. Radiometric dates were provided by J. v. d. P. L. J. L. wrote the manuscript with specific contributions from M. H. M. G. and E. T. and additional comments from H. H. and M. Z. All Fúquene project members contributed their expertise to succeed the project.

## References

Alfonso, J. A., Martínez, M., Flores, S., and Benzo, T., Distribution of trace elements in offshore sediments of the Orinoco Delta, J. Coast. Res., 22, 502–510, 2006.

Baisch, S. and Bokelmann, G. H. R.: Spectral analysis with incomplete time series: an example from seismology, Comput. Geosci., 25, 739–750, 1999.

Baker, P. A., Rigsby, C. A., Seltzer, G. O., Fritz, S. C., Lowenstein, T. K., Bacher, N. P., and Veliz, C.: Tropical climate changes at millennial and orbital timescales on the Bolivian Altiplano, Nature, 409, 698–701, 2001.

Balan, E., Patrick, T., Jupille, J., Fritsch, E., Mueller, J. P., and Calas, G.: Surface chemistry of weathered Zircon, Chem. Geol., 181, 13–22, 2001.

Bintanja, R., v. d. Wal, R. S. W., and Oerlemans, J.: Modelled atmospheric temperatures and global sea levels over the past million years, Nature, 437, 125–128, 2005.

Blackman, R. B. and Tuckey, J. W.: The measurement of power spectra from the point of view of communication engeneering, Dover publications, New York, 1958.

Blanchon, P., Eisenhauer, A., Fietzke, J., and Liebetrau, V.: Rapid sea-level rise and reef back-stepping at the close of the last interglacial highstand, Nature, 458, 881–885, 2009.

Bond, G., Broecker, W., Johnsen, S., McManus, J., Labeyrie, L., Jouzel, J., and Bonani, G.: Correlations between climate record from North Atlantic sediments and Greenland ice, Nature, 365, 143–147, 1993.

Broecker, W. S.: Massive iceberg discharges as triggers for global climate change, Nature, 372, 421–424, 1994.

Brovkin, V., Ganopolski, A., and Svirezhev, Y.: A continuous climate-vegetation classification for use in climate-biosphere studies, Ecol. Model., 101, 251–261, 1997.

Calov, R., Ganopolski, A., Claussen, M., Petoukhov, V., and Greve, R.: Transient simulation of the last glacial inception, Part I: Glacial inception as a bifurcation of the climate system, Clim. Dynam., 24, 545–561, 2005a.

Calov, R., Ganopolski, A., Petoukhov, V., Claussen, M., Brovkin, V., and Kubatzki, C.: Transient simulation of the last glacial inception, Part II: Sensitivity and feedback analysis, Clim. Dynam., 24, 563–576, 2005b.

Cane, M. and Clement, A. C.: A role for the tropical Pacific coupled ocean-atmosphere system on Milankovitch and millennial timescales Part II: Global Impacts, Geophys. Monogr., 112, 373–383, 1999.

Cheng, H., Edwards, R. L., Broecker, W. S., Denton, G. H., Kong, X., Wang, Y., Zhang, R., and Wang, X.: Ice age Terminations, Science, 326, 248–252, 2009.

Cheng, H., Edwards, R. L., Wang, Y., Kong, X., Ming, Y., Kelly, M. J., Wang, X., Gallup, C. D., and Liu, W.: Penultimate glacial monsoon record from Hulu Cave and two-phase glacial terminations, Geology, 34, 217–220, 2006.

Chiang, J. C. H., Biasutti, M., and Battisti, D. S.: Sensitivity of the Atlantic Intertropical Convergence Zone to Last Glacial Maximum boundary conditions, Paleoceanography, 18, 1–18, 2003.

Claussen, M., Kubatzki, C., Brovkin, V., Ganopolski, A., Hoelzmann, P., and Pachur, H.-J.: Simulation of an abrupt change in Saharan vegetation in the mid-Holocene, Geophys. Res. Lett., 26, 2037–2040, 1999.

Clement, A. C. and Peterson, L. C.: Mechanisms of abrupt climate change of the last glacial period, Rev. Geophys., 46, RG4002, doi:10.1029/2006RG000204, 2008.

Davidson, W.: Iron and manganese in lakes, Earth Sci. Rev., 34, 119–163, 1993.

Denton, G. H., Alley, R. B., Comer, G. C., and Broecker, W. S.: The role of seasonality in abrupt climate change, Quaternary Sci. Rev., 24, 1159–1182, 2005.

Florez, A.: Relacion altitidinal de la temperature del suelo y del aire en los Andes centrales de Colombia, Colombia Geografica, 12, 5–38, 1986.

Flückinger, J., Monnin, E., Stauffer, B., Schwander, J., Stocker, T. F., Chappelaz, J., Raynaud, D., and Barnola, J.-M., High resolution Holocene $N_2O$ ice core record and its relationship with $CH_4$ and $CO_2$, Global Biogechem. Cy., 6, GB1010, doi:10.29/2001GB001417, 2002.

Gallup, C. D., Cheng, H., Taylor, F. W., and Edward, R. L.: Direct determination of the timing of sea level change during Termination II, Science, 295, 310–313, 2002.

Ganopolski, A. and Rahmstorf, S.: Rapid changes of glacial climate simulated in a coupled climate model, Nature, 409, 153–158, 2001.
Ganopolski, A., Rahmstorf, S., Petoukhov, V., and Claussen, M.: Simulation of modern and glacial climates with a coupled global model of intermediate complexity, Nature, 391, 351–356, 1998.
GAVESA: Perforaciones en agua Laguna de Fúquene, Departamento de Cundinamarca, 2002.
González, C., Dupont, L. M., Behling, H., and Wefer, G.: Neotropical vegetation response to rapid climate changes during the last glacial period: Palynological evidence from the Cariaco Basin, Quaternary Res., 69, 217–230, 2008.
GRIP-Members: Climate instability during the last interglacial period recorded in the GRIP ice core, Nature, 364, 203–207, 1993.
Grootes, P. M., Stuiver, M., White, J. W. C., Johnsen, S., and Jouzel, J.: Comparison of oxygen isotopes records from the GISP2 and GRIP Greenland ice cores, Nature, 366, 552–554, 1993.
Heslop, D., and Dekkers, M. J., Spectral analysis of unevenly spaced climatic time series using CLEAN: signal recovery and derivation of significance levels using Monte Carlo simulation. Physics of the Earth and Planetary Interiors, 130, 103-116 (2002).
Hessler, I., Dupont, L. M., Bonnefille, R., Behling, H., González, C., Helmens, K. F., Hooghiemstra, H., Lebamba, J., Ledru, M.-P., Lézine, A.-M., Maley, J., Marret, F., and Vincens, A.: Millennial-scale changes in vegetation records from tropical Africa and South America during the last glacial, Quaternary Sci. Rev., 29(21–22), 2882–2899, 2010.
Hooghiemstra, H.: Vegetational and climatic history of the high plain of Bogotá, Colombia, J. Cramer, Vaduz. Dissertationes Botanicae, 79, 368 pp., 1984.
Hooghiemstra, H., Melice, J. L., Berger, A., and Shackleton, N.: Frequency spectra and paleoclimatic variability of the high-resolution 30 1450 ka Funza I pollen record (Eastern Cordillera, Colombia), Quaternary Sci. Rev., 12, 141–156, 1993.
Hooghiemstra, H. and Van der Hammen, T., Late Quaternary vegetation history and paleoecology of Laguna Pedro Palo (subandean forest belt, Eastern Cordillera, Colombia, Rev. Palaeobot. Palyno., 77, 235–262, 1993.
Imbrie, J., Hays, J. D., Martinson, D. G., McIntyre, A., Mix, A. C., Morley, J. J., Pisias, N. G., Prell, W. L., and Shackleton, N. J.: The orbital theory of Pleistocene climate: support from a revised chronology of the marine $\delta$18O record, in: Milankovitch and Climate, understanding the response to astronomical forcing, edited by: Berger, A., Imbrie, J., Hays, J., Kukla,

G., and Saltzman, B., NATO Advanced Science Institute Series C 126, Reidel Publishing Company, Dordrecht/Boston/Lancaster, 1984.

Imbrie, J. and Imbrie, J. Z.: Modelling the climatic response to orbital variations, Science, 207, 943–952, 1980.

Jansen, J. H. F., Van der Gaast, S. J., Koster, B., and Vaars, A. J.: CORTEX, a shipboard XRF-scanner for element analyses in split sediment cores, Mar. Geol., 151, 143–153, 1998.

Jouzel, J., Masson-Delmotte, V., Cattani, O., Dreyfus, G., Falourd, S., Hoffmann, G., Minster, B., Nouet, J., Barnola, J. M., Chappellaz, J., Fischer, H., Gallet, J. C., Johnsen, S., Leuenberger, M., Loulergue, L., Luethi, D., Oerter, H., Parrenin, F., Raisbeck, G., Raynaud, D., Schilt, A., Schwander, J., Selmo, E., Souchez, R., Spahni, R., Stauffer, B., Steffensen, J. P., Stenni, B., Stocker, T. F., Tison, J. L., Werner, M., and Wolff, E. W.: Orbital and millennial Antarctic climate variability over the past 800,000 years, Science, 317, 793–797, 2007.

Klein, A. G., Seltzer, G. O., and Isacks, B. L.: Modern and last local glacial maximum snowlines in the Central Andes of Peru, Bolivia, and Northern Chile, Quaternary Sci. Rev., 18, 63–84, 1999.

Landais, A., Chappellaz, J., Delmotte, M., Jouzel, J., Blunier, T., Bourg, C., Caillon, N., Cherrier, S., Malaize, B., Masson-Delmotte, V., Raynaud, D., and Schwander, J.: A tentative reconstruction of the last interglacial and glacial inception in Greenland based on new gas measurements in the Greenland Ice Core Project (GRIP) ice core, J. Gepphys. Res., 108(D18), 4563, doi:10.1029/2002JD003147, 2003.

Lashof, D. A.: The use of global warming potentials in the Kyoto Protocol, Climatic Change, 44, 423–425, 2000.

Lea, D. W., Pak, D. K., and Spero, H. J.: Climate impact of late Quaternary equatorial Pacific sea surface temperature variations, Science, 289, 1719–1724, 2000.

Leduc, G., Vidal, L., Tachikawa, K., Rostek, F., Sonzogni, C., Beaufort, L., and Bard, E.: Moisture transport across Central America as a positive feedback on abrupt climatic changes, Nature, 445, 908–911, 2007.

Lisiecki, L. E. and Raymo, M. E.: A Pliocene-Pleistocene stack of 57 globally distributed benthic $\delta^{18}O$ records, Paleoceanography, 20, PA1003, doi:10.1029/2004PA001071, 2005.

Locarnini, R. A., Mishonov, A. V., Antonov, J. L., Boyer, T. P., and Garcia, H. E.: Temperature, in: World Ocean Atlas 2005, edited by: Levitus, S., US Government Printing Office, Washington, DC, 182 pp., 2006.

Martrat, B., Grimalt, J. O., Shackleton, N., De Abreu, L., Hutterli, M. A., and Stocker, T. F.: Four climate cycles of recurring deep and surface water destabilizations on the Iberian Margin, Science, 317, 502–507, 2007.

Members, E. C.: One-to-one coupling of glacial climate variability in Greenland and Antarctica, Nature, 444, 196–198, 2006.

Mommersteeg, H.: Vegetation development and cyclic and abrupt climatic change during the Late Quaternary, Unpublished Ph.D. thesis, University of Amsterdam, 1998.

Mudelsee, M.: TAUEST: a computer program for estimating persistence in unevenly spaced weather/climate time series, Comput. Geosci., 28, 69–72, 2002.

North GRIP ice core project members (NGRIP): High-resolution record of Northern Hemisphere climate extending into the last interglacial period, Nature, 431, 147–151, 2004.

Nyakairu, G. W. A. and Koeberl, C.: Variation of mineral, chemical, and rare earth element composition in size fractions of clay-rich sediments from the Kajjansi and Ntawo clay deposits, Chem. Erde, 62, 73–86, 2002.

Paillard, D., Labeyrie, L., and Yiou, P.: Macintosh program performs time-series analysis, EOS, 77, 379, 1996.

Parrenin, F., Barnola, J.-M., Beer, J., Blunier, T., Castellano, E., Chappellaz, J., Dreyfus, G., Fischer, H., Fujita, S., Jouzel, J., Kawamura, K., Lemieux-Dudon, B., Loulergue, L., Masson-Delmotte, V., Narcisi, B., Petit, J.-R., Raisbeck, G., Raynaud, D., Ruth, U., Schwander, J., Severi, M., Spahni, R., Steffensen, J. P., Svensson, A., Udisti, R., Waelbroeck, C., and Wolff, E.: The EDC3 chronology for the EPICA Dome C ice core, Clim. Past, 3, 485–497, doi:10.5194/cp-3-485-2007, 2007.

Peltier, W. R.: Global glacial isostasy and the surface of the ice-age earth: The ICE-5G (VM2) model and GRACE, Annu. Rev. Earth Pl. Sc., 32, 111–149, 2004.

Peterson, L. C., Haug, G. H., Hughen, K. A., and Rohl, U., Rapid changes in the hydrologic cycle of the tropical Atlantic during the last glacial, Science, 290, 1947–1951, 2000.

Petit, J. R., Jouzel, J., Raynaud, D., Barkov, N. I., Barnola, J. M., Basile, I., Bender, M., Chappellaz, J., Davis, M., Delaygue, G., Delmotte, M., Kotlyakov, V. M., Legrand, M., Lipenkov, V. Y., Lorius, C., Pepin, L., Ritz, C., Saltzman, E., and Stievenard, M.: Climate and atmospheric history of the past 420,000 years from the Vostok ice core, Antarctica, Nature, 399, 429–436, 1999.

Petoukhov, V., Ganopolski, A., Brovkin, V., Claussen, M., Eliseev, A., Kubatzki, C., and Rahmstorf, S.: CLIMBER-2: a climate system model of intermediate complexity, Part I: model





CPD
6, 2117–2158, 2010

description and performance for present climate, Clim. Dynam., 16, 1–17, 2000.
Richter, T. O., van der Gaast, S., Koster, B., Vaasrs, A., Gieles, R., de Stigter, H. C., de Haas, H., van Weering, T. C. E., and Rothwell, R. G.: The Avaatech XRF Core Scanner: technical description and applications to NE Atlantic Sediments, in: New Techniques in Sediment Core Analysis, anonymous, editors, Geological Society, London, Special Publications, The Geological Society of London, London, 39–50, 2006.
Roberts, D. H., Lehar, J., and Dreher, J. W.: Time series analysis with ClEAN – Part One – derivation of a spectrum, Astron. J., 93, 968–989, 1987.
Robertson, A., Overpeck, J., Rind, D., Mosley-Thompson, E., Zielinski, G., Lean, J., Koch, D., Penner, J., and Tegen, I.: Hypothesized climate forcing time series for the last 500 years, J. Geophys. Res.-Atmos., 106, 14783–14803, 2001.
Sarmiento, G., Gaviria, S., Hooghiemstra, H., Berrio, J. C., and Van der Hammen, T.: Landscape evolution and origin of Lake Fúquene (Colombia): tectonics, erosion and sedimentation processes during the Pleistocene, Geomorphology, 100, 563–575, 2008.
Schulz, M. and Mudelsee, M.: REDFIT: estimating red-noise spectra directly from unevenly spaced paleoclimatic time series, Comput. Geosci., 28, 421–426, 2002.
Stiles, C. A., Mora, C., and Driese, S. G.: Pedogenic processes and domain boundaries in a vertisol climosequence: evidence from titanium and zirconium distribution and morphology, Geoderma, 116, 279–299, 2003.
Stocker, T. F., Wright, D. G., and Mysak, L. A.: A zonally averaged, coupled ocean-atmosphere model for paleoclimate studies, J. Climate, 5, 773–797, 1992.
Stuiver, P., Reimer, J., and Reimer, R.: CALIB radiocarbon calibration, Execute version 5.0.2html (2005), http://calib.org, last access: 22 Ocotber 2009.
Svensson, A., Andersen, K. K., Bigler, M., Clausen, H. B., Dahl-Jensen, D., Davies, S. M., Johnsen, S. J., Muscheler, R., Parrenin, F., Rasmussen, S. O., Röthlisberger, R., Seierstad, I., Steffensen, J. P., and Vinther, B. M.: A 60 000 year Greenland stratigraphic ice core chronology, Clim. Past, 4, 47–57, doi:10.5194/cp-4-47-2008, 2008.
Thompson, W. G. and Goldstein, S. L.: A radiometric calibration of the SPECMAP timescale, Quarternary Sci. Rev., 25, 3207–3215, 2006.
Torres, V., Vandenberghe, J., and Hooghiemstra, H.: An environmental reconstruction of the sediment infill of the Bogotá basin (Colombia) during the last 3 million years from abiotic and biotic proxies, Palaeogeogr. Palaeoclim. Palaeoecol., 226, 127–148, 2005.

Tuenter, E., Weber, S. L., Hilgen, F. J., Lourens, L. J., and Ganopolski, A.: Simulation of climate phase lags in response to precession and obliquity forcing and the role of vegetation, Clim. Dynam., 24, 279–295, 2005.

Urrutia, R. and Vuille, M.: Climate change projections for the tropical Andes using a regional climate model: Temperature and precipitation simulations for the end of the 21st century, J. Geophys. Res., 114, D02108, doi:10.1029/2008JD011021, 2009.

Van't Veer, R. and Hooghiemstra, H.: Montane forest evolution during the last 650 000 yr in Colombia: a multivariate approach based on pollen record Funza-I, J. Quaternary Sci., 15, 329–346, 2000.

Van't Veer, R., Ran, R., Mommersteeg, E. T. H., and Hooghiemstra, H. J. P. M.: Multivariate analysis of the Middle and Late Pleistocene Funza pollen records of Colombia, Mededelingen Rijks Geologische Dienst, 52, 195–212, 1995.

Van der Hammen, T.: The Pleistocene changes of vegetation and climate in tropical South America, J. Biogeogr., 1, 3–26, 1974.

Van der Hammen, T., and González, E.: Upper Pleistocene and Holocene climate and vegetation of the Sabana de Bogotá, Leidse Geologische Mededelingen, 25, 261–315, 1960.

van Geel, B. and van der Hammen, T.: Upper Quaternary vegetational and climatic sequence of the Fúquene area Eastern Cordillera, Colombia, Palaeogeogr. Palaeoclim. Palaeoecol., 14, 9–92, 1973.

Wang, X. F., Auler, A. S., Edwards, R. L., Cheng, H., Cristalli, P. S., Smart, P. L., Richards, D. A., and Shen, C. C.: Wet periods in northeastern Brazil over the past 210 kyr linked to distant climate anomalies, Nature, 432, 740–743, 2004.

Wang, Y., Cheng, H., Edwards, R. L., Kong, X., Shao, X., Chen, S., Wu, J., Jiang, X., Wang, X., and An, Z.: Millennial- and orbital-scale changes in the East Asian monsoon over the past 224,000 years, Nature, 451, 1090–1093, 2008.

Wille, M., Hooghiemstra, H., Behling, H., van der Borg, K., and Negret, A. J.: Environmental change in the Colombian subandean forest belt from 8 pollen records: the last 50 kyr, Veg. Hist. Archaeobot., 10, 61–77, 2001.

Ziegler, M., Nurnberg, D., Karas, C., Tiedemann, R., and Lourens, L. J.: Persistent summer expansion of the Atlantic Warm Pool during glacial abrupt cold events, Nat. Geosci., 1, 601–605, 2008.

**Table 1.** Core sections (depth in cm) of Fúquene-9 and Fúquene-10.

| Fúquene-9 | Fúquene-10 | Fúquene-9 | Fúquene-10 |
|---|---|---|---|
| | 6799–6702 | | 3259–3161 |
| | 6644–6546 | 3199–3101 | |
| | 6499–6402 | | 3140–3041 |
| | 6379–6282 | 3079–2981 | |
| | 6259–6162 | | 3019–2921 |
| 6199–6100 | | 2959–2861 | |
| | 6139–6043 | | 2899–2802 |
| 6079–5981 | | 2838–2742 | |
| | 6019–5922 | | 2779–2681 |
| 5960–5861 | | 2719–2620 | |
| | 5899–5801 | | 2649–2556 |
| 5839–5741 | | 2599–2501 | |
| | 5778–5681 | | 2539–2441 |
| 5719–5621 | | 2479–2381 | |
| | 5659–5561 | | 2419–2321 |
| 5599–5501 | | 2359–2261 | |
| | 5538-5441 | | 2299–2201 |
| 5479-5380 | | 2239-2146 | |
| | 5415–5321 | | 2179–2083 |
| 5350–5261 | | 2119–2021 | |
| | 5299–5202 | | 2059–1965 |
| 5239–5163 | | 1999–1901 | |
| | 5179–5082 | | 1939–1841 |
| 5119–5020 | | 1879–1781 | |
| | 5059–4962 | | 1819–1721 |
| 4999–4901 | | 1759–1661 | |
| | 4939–4842 | | 1698–1601 |
| 4878–4781 | | 1639–1541 | |





CPD
6, 2117–2158, 2010

Rapid shifts in South American montane climates over the past 284 000 years

M. H. M. Groot et al.

**Table 1.** Continued.

| Fúquene-9 | Fúquene-10 | Fúquene-9 | Fúquene-10 |
|---|---|---|---|
| | 4819–4721 | | 1579–1480 |
| 4758–4660 | | 1519–1421 | |
| | 4699-4600 | | 1459–1361 |
| 4639–4541 | | 1399–1301 | |
| | 4579-4481 | | 1339–1241 |
| 4521–4422 | | 1279–1181 | |
| | 4459–4360 | | 1219–1121 |
| 4399–4301 | | 1159–1061 | |
| | 4339–4241 | | 1099–1001 |
| 4279–4181 | | 1039–941 | |
| | 4216–4122 | | 970–880 |
| 4159–4061 | | 919–821 | |
| | 4099–4001 | | 859–760 |
| 4038–3941 | | 799–701 | |
| | 3949–3879 | | 739–641 |
| 3919–3820 | | 679–580 | |
| | 3859–3761 | | 619–521 |
| 3798–3701 | | 559–460 | |
| | 3738–3641 | | 499–401 |
| 3679–3582 | | 439–341 | |
| | 3619–3521 | | 379–280 |
| 3559–3461 | | 318–220 | |
| | 3499–3400 | | 259–160 |
| 3439–3341 | | 199–167 | |
| | 3378-3281 | | 140–100 |
| 3319–3220 | | | |





CPD
6, 2117–2158, 2010

**Table 2.** Tie points between Fúquene-9 and Fúquene-10.

| Fq-10 depth (cm) | Fq-9 depth (cm) | Offset (cm) |
|---|---|---|
| 169 | 108 | 61 |
| 257 | 196 | 61 |
| 378 | 318 | 60 |
| 499 | 437 | 62 |
| 737 | 669 | 68 |
| 858 | 793 | 65 |
| 969 | 899 | 70 |
| 1338 | 1255 | 83 |
| 1458 | 1368 | 90 |
| 1578 | 1475 | 103 |
| 1698 | 1587 | 111 |
| 1818 | 1742 | 76 |
| 2297 | 2212 | 85 |
| 2370 | 2279 | 91 |
| 2418 | 2367 | 51 |
| 2537 | 2522 | 15 |
| 2648 | 2695 | −47 |
| 2778 | 2803 | −25 |
| 2898 | 2915 | −17 |
| 3018 | 3065 | −47 |
| 3139 | 3170 | −31 |
| 3257 | 3286 | −29 |
| 3377 | 3418 | −41 |
| 3498 | 3543 | −45 |
| 3618 | 3649 | −31 |
| 3738 | 3768 | −30 |
| 3858 | 3895 | −37 |
| 3948 | 3992 | −44 |
| 4097 | 4145 | −48 |





CPD
6, 2117–2158, 2010

**Table 2.** Continued.

| Fq-10 depth (cm) | Fq-9 depth (cm) | Offset (cm) |
|---|---|---|
| 4213 | 4260 | −47 |
| 4338 | 4374 | −36 |
| 4457 | 4492 | −35 |
| 4578 | 4614 | −36 |
| 4697 | 4742 | −45 |
| 4817 | 4871 | −54 |
| 4938 | 4970 | −32 |
| 5057 | 5092 | −35 |
| 5297 | 5327 | −30 |
| 5324 | 5369 | −45 |





CPD
6, 2117–2158, 2010

**Table 3.** Selected intervals used to construct the Fúquene-9 composite record.

| Fq-9 Depth (cm) | Fq-10 Depth (cm) | *Fq-10 drilling depth* | Fq-9 Depth (cm) | Fq-10 Depth (cm) | *Fq-10 drilling depth* |
|---|---|---|---|---|---|
| 6000–5982 | | | 2719–2620 | | |
| 5959–5866 | | | 2599–2516 | | |
| 5839–5824 | | | | 2515–2480 | *2530–2495* |
| | 5823–5736 | *5778–5691* | 2479–2381 | | |
| 5719–5622 | | | 2359–2269 | | |
| 5599–5584 | | | | 2268–2240 | *2359–2331* |
| | 5583–5489 | *5538–5444* | 2239–2146 | | |
| 5479–5461 | | | 2119–2090 | | |
| | 5460–5370 | *5415–5325* | 2083–2021 | | |
| 5350–5329 | | | 1999–1901 | | |
| | 5328–5235 | *5298–5205* | 1879–1819 | | |
| | 5208–5114 | *5178–5084* | | 1816–1795 | *1901–1880* |
| | 5094–5001 | *5059–4966* | 1794–1781 | | |
| | 4971–4878 | *4939–4846* | 1758–1695 | | |
| | 4873–4780 | *4819–4726* | | 1694–1645 | *1770–1721* |
| 4758–4744 | | | 1639–1571 | | |
| | 4743–4645 | *4698–4600* | | 1570–1490 | *1681–1601* |
| 4639–4615 | | | 1489–1470 | | |
| | 4614–4521 | *4578–4485* | | 1469–1389 | *1572–1492* |
| 4520–4426 | | | 1388–1369 | | |
| | 4425–4400 | *4390–4365* | | 1368–1280 | *1458–1370* |
| 4399–4312 | | | 1278–1257 | | |
| 4278–4245 | | | | 1256–1160 | *1339–1243* |
| | 4244–4170 | *4197–4123* | 1158–1062 | | |
| 4158–4065 | | | | 1061–1039 | *1144–1122* |
| | 4064–4049 | *4016–4001* | 1038–941 | | |
| 4037–3994 | | | | 899–810 | *969–880* |
| | 3993–3923 | *3949–3879* | 799–739 | | |

**Table 3.** Continued.

| Fq-9 Depth (cm) | Fq-10 Depth (cm) | *Fq-10 drilling depth* | Fq-9 Depth (cm) | Fq-10 Depth (cm) | *Fq-10 drilling depth* |
|---|---|---|---|---|---|
| 3919–3896 | | | | 738–695 | *803–760* |
| | 3895–3799 | *3858–3762* | 679–580 | | |
| | 3768–3679 | *3738–3649* | 558–460 | | |
| 3678–3596 | | | | 437–339 | *499–401* |
| | 3595–3564 | *3564–3533* | | 319–227 | *379–287* |
| 3558–3499 | | | 199–167 | | |
| | 3498–3450 | *3453–3405* | | | |
| 3438–3342 | | | | | |
| 3318–3260 | | | | | |
| | 3259–3199 | *3230–3170* | | | |
| 3198–3104 | | | | | |
| 3077–2981 | | | | | |
| 2958–2861 | | | | | |
| | 2860–2838 | *2843–2821* | | | |
| 2837–2742 | | | | | |

Core depth of Fúquene-9 are according to the original depth intervals. Core depth of Fúquene-10 are shown as their original depth intervals and the new depth intervals after correlating the cores.





CPD
6, 2117–2158, 2010

**Table 4.** Tie points between Fq-2, Fq-7C and Fq-9C.

| Depth (cm) Fq-7C | Age tie points | Reference |
|---|---|---|
| 280.00 | 2.00 | Revised $^{14}$C age from Fq-7C |
| 349.00 | 6.890 | Revised $^{14}$C age from Fq-7C |
| 403.00 | 7.890 | Revised $^{14}$C age from Fq-7C |
| 448.00 | 8.570 | Revised $^{14}$C age from Fq-7C |
| 467.00 | 8.620 | Revised $^{14}$C age from Fq-7C |
| 481.00 | 8.680 | Revised $^{14}$C age from Fq-7C |
| 491.00 | 8.950 | Revised $^{14}$C age from Fq-7C |
| 504.00 | 9.600 | Revised $^{14}$C age from Fq-7C |
| 521.00 | 15.500 | Revised $^{14}$C age from Fq-7C |
| 543.00 | 17.000 | Revised $^{14}$C age from Fq-7C |
| 651.00 | 21.300 | Revised $^{14}$C age from Fq-7C |
| 699.00 | 23.650 | Revised $^{14}$C age from Fq-7C |
| 915.00 | 35.074 | Matching maxima in AP (related to maxima in *Alnus*, *Quercus* and *Podocarpus*) between Fq-9C and Fq-7C |
| 1205.00 | 53.375 | Matching maxima in AP (related to maxima in *Alnus*, *Myrica* and *Quercus*) between Fq-9C and Fq-7C |
| 1530.00 | 70.071 | Matching maxima in AP (related to maxima in *Quercus*) between Fq-9C and Fq-7C |
| **Depth (cm) Fq-2** | **Age tie points** | **Reference** |
| 6.25 | 0.00 | Revised $^{14}$C age from Fq-2 |
| 320.00 | 6.78 | Revised $^{14}$C age from Fq-2 |
| 385.00 | 8.47 | Revised $^{14}$C age from Fq-2 |
| 465.00 | 10.90 | Revised $^{14}$C age from Fq-2 |
| 490.00 | 12.80 | Revised $^{14}$C age from Fq-2 |
| 508.00 | 13.55 | Revised $^{14}$C age from Fq-2 |





CPD
6, 2117–2158, 2010

**Table 5.** Ice areas and ice heights.

| Gridbox American Icesheet | Land fraction | Ice fraction | Height (in $H_{am}$) |
|---|---|---|---|
| 160° W–110° W; 60° N–70° N | 1 | 0.5 | 0.5 |
| 160° W–110° W; 50° N–60° N | 0.2 | 1 | 0.5 |
| 110° W–60° W; 70° N–80° N | 0.7 | 1 | 0.5 |
| 110° W–60° W; 60° N–70° N | 0.7 | 1 | 1 |
| 110° W–60° W; 50° N–60° N | 1 | 1 | 1 |
| 110° W–60° W; 40° N–50° N | 1 | 0.5 | 0.5 |
| **Gridbox Eurasian Icesheet** | **Land fraction** | **Ice fraction** | **Height (in $H_{eur}$)** |
| 10° W–40° E; 70° N–80° N | 0.9 | 1 | 1 |
| 10° W–40° E; 60° N–70° N | 0.9 | 1 | 1 |
| 10° W–40° E; 50° N–60° N | 1 | 0.5 | 0.5 |
| 40° E–90° E; 70° N–80° N | 0.9 | 1 | 1 |
| 40° E–90° E; 60° N–70° N | 1 | 0.5 | 1 |



Discussion Paper | Discussion Paper | Discussion Paper | Discussion Paper |

CPD

6, 2117–2158, 2010

Rapid shifts in South American montane climates over the past 284 000 years

M. H. M. Groot et al.

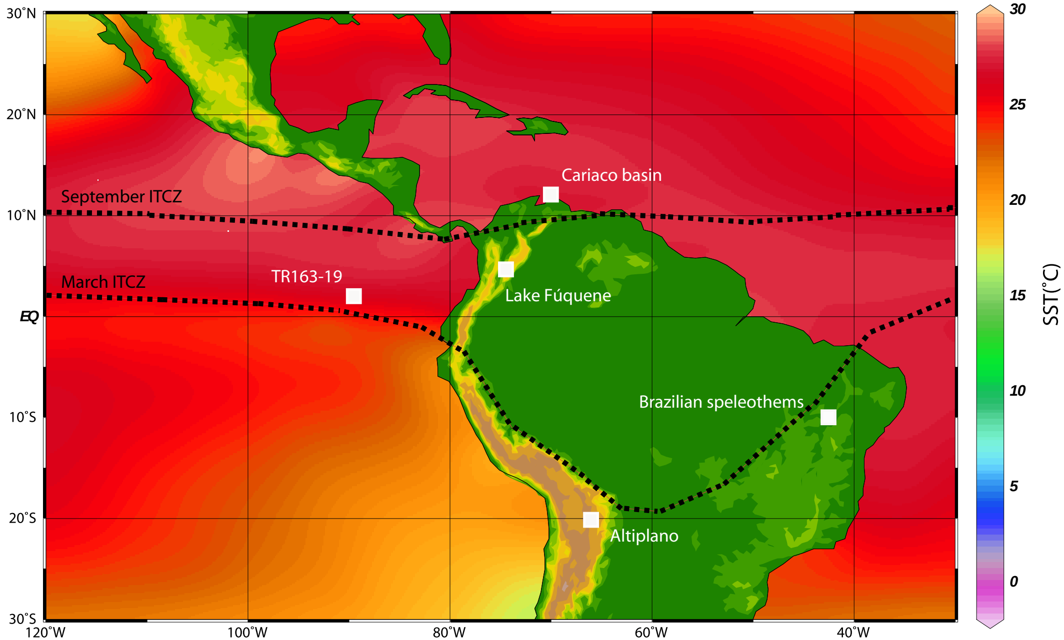


**Fig. 1.** Current annual mean sea surface temperature (SST) (Locarnini et al., 2006) and generalized position of the inter tropical convergence zone (ITCZ) during March and September. Location of sites: Lake Fúquene (5°28′ N, 73°45′ W; 2580 m a.s.l. – above sea-level, Colombia), TR163-19 (2°15.5′ N, 90°57.1′ W; 2348 m water depth, equatorial Pacific) (Lea et al., 2000), MD03-2622 (10°42.69′ N, 65°10.15′ W; 877 m water depth, Cariaco Basin) (González et al., 2008), Brazilian speleothem (10°10′ S, 40°50′ W; 500 m a.s.l.) (Wang et al., 2004), and Bolivian Altiplano (20°14.97′ S, 67°30.03′ W; 3653 m a.s.l.) (Baker et al., 2001).





CPD
6, 2117–2158, 2010

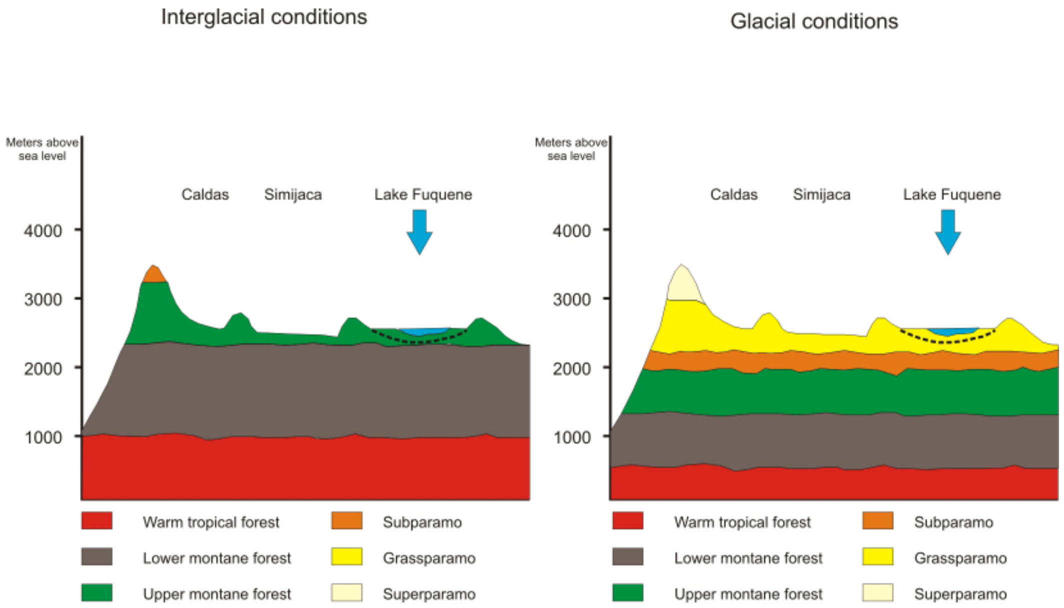


**Fig. 2.** Distribution pattern of source areas of pollen taxa during full glacial conditions and modern (interglacial) times.





CPD
6, 2117–2158, 2010

Rapid shifts in South American montane climates over the past 284 000 years

M. H. M. Groot et al.

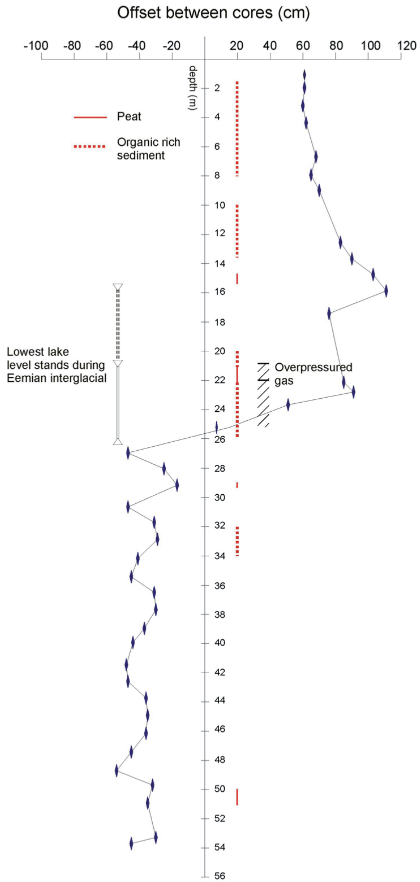


**Fig. 3.** Graph of downcore changes in the offset between core Fúquene-9 and Fúquene-10. Blue ellipses represent the tie points as indicated in Table 2. Gaps between vertical red lines represent mineral-rich sediments.





CPD
6, 2117–2158, 2010

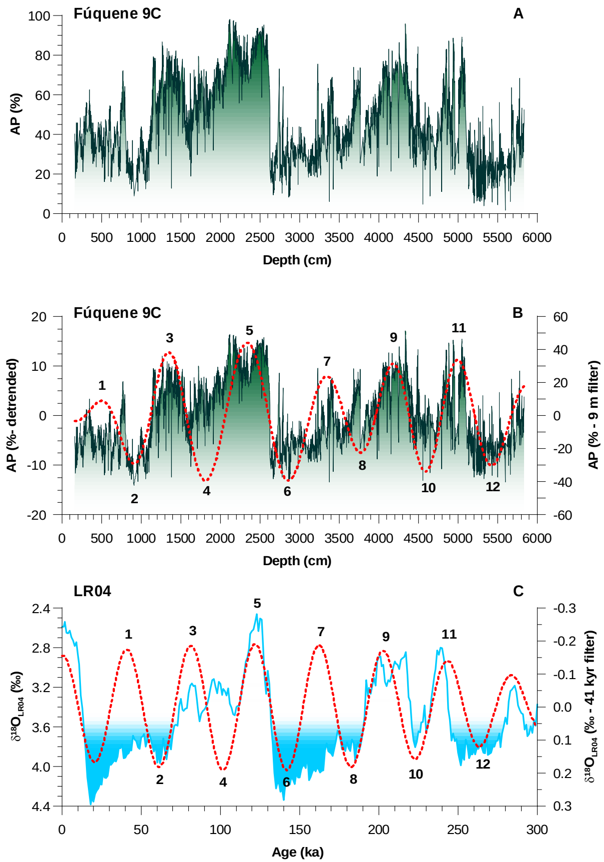


**Fig. 4.** The AP% data series of core Fq-9C plotted on a depth scale. **(A)** Raw data. **(B)** Detrended and interpolated depth series overlain by a Gaussian filter centered at 0.0011 ± 0.0004 (i.e., ~9 m component). **(C)** Correlation of the 41-kyr related component in the AP% depth series of core Fq-9C to that of the LR04 benthic oxygen isotope stack (see text for explanations and references).





CPD
6, 2117–2158, 2010

Rapid shifts in South American montane climates over the past 284 000 years

M. H. M. Groot et al.

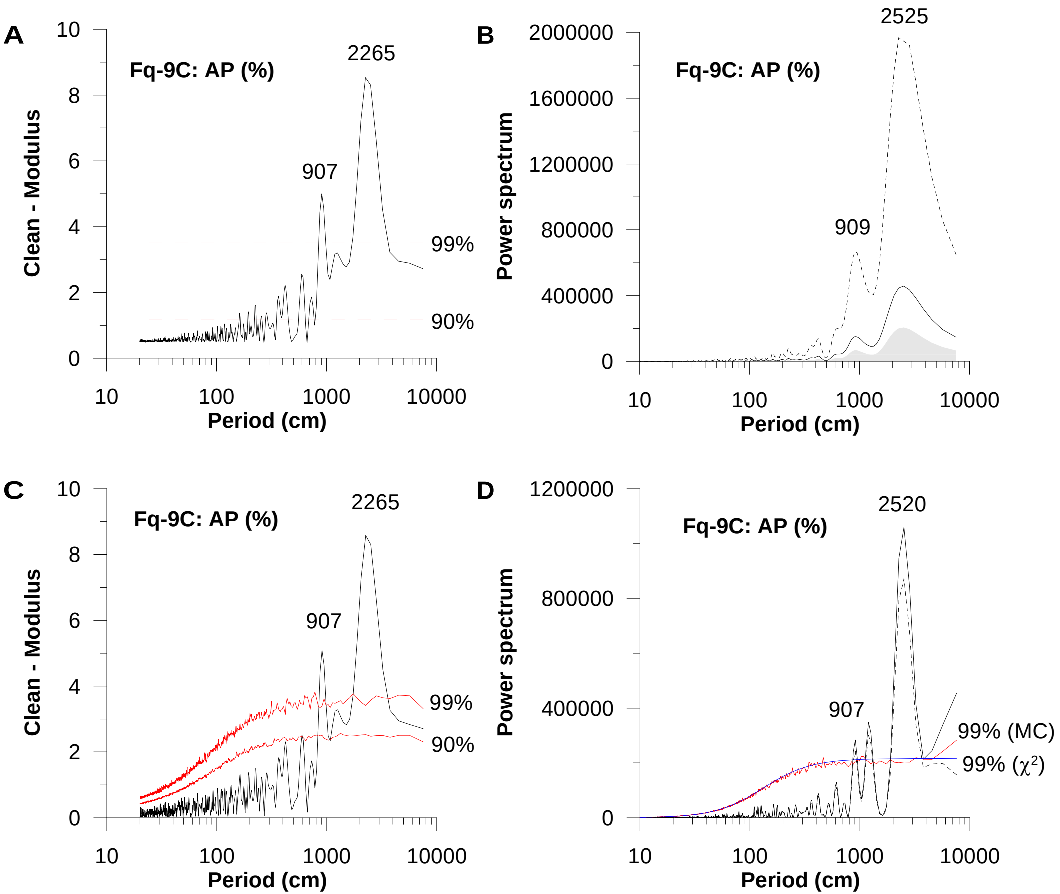


**Fig. 5.** Spectral analysis results of the AP% data series of core Fq-9C. **(A)** CLEAN. **(B)** Blackman-Tukey. **(C)** CLEAN (emended). **(D)** REDFIT (see text for explanations and references).





CPD
6, 2117–2158, 2010

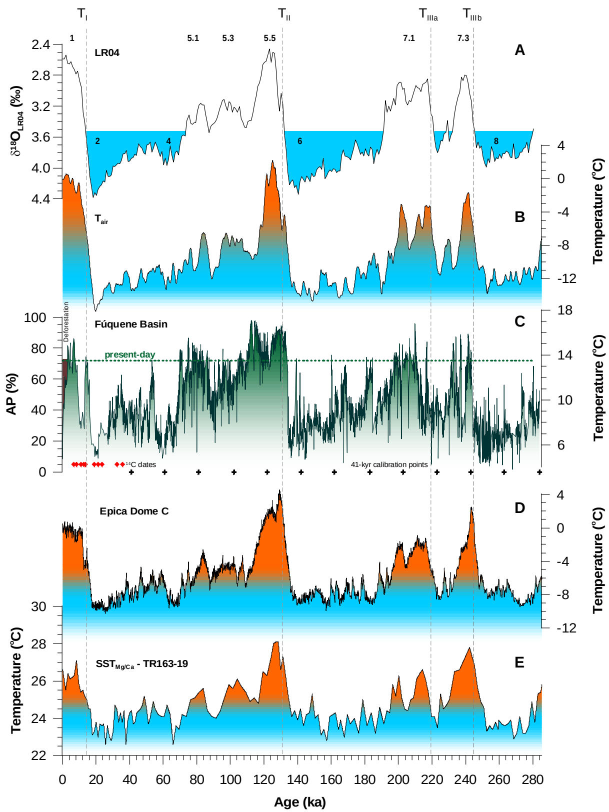


**Fig. 6.** Comparison of mean annual temperature (MAT) changes at Lake Fúquene with other records. **(A)** LR04 benthic $\delta^{18}$O stack (Lisiecki and Raymo, 2005). **(B)** Modeled NH air temperatures (Bintanja et al., 2005). **(C)** AP%-based MAT at Lake Fúquene. **(D)** The deuterium-based temperature record of Epica Dome C (Jouzel et al., 2007; Parrenin et al., 2007). **(E)** Mg/Ca-derived sea surface temperature (SST) record of TR163-19 (Lea et al., 2000). The numbers in (A) indicate Marine Isotope Stages. Brown shaded area in (C) represents deforestation interval.





CPD
6, 2117–2158, 2010

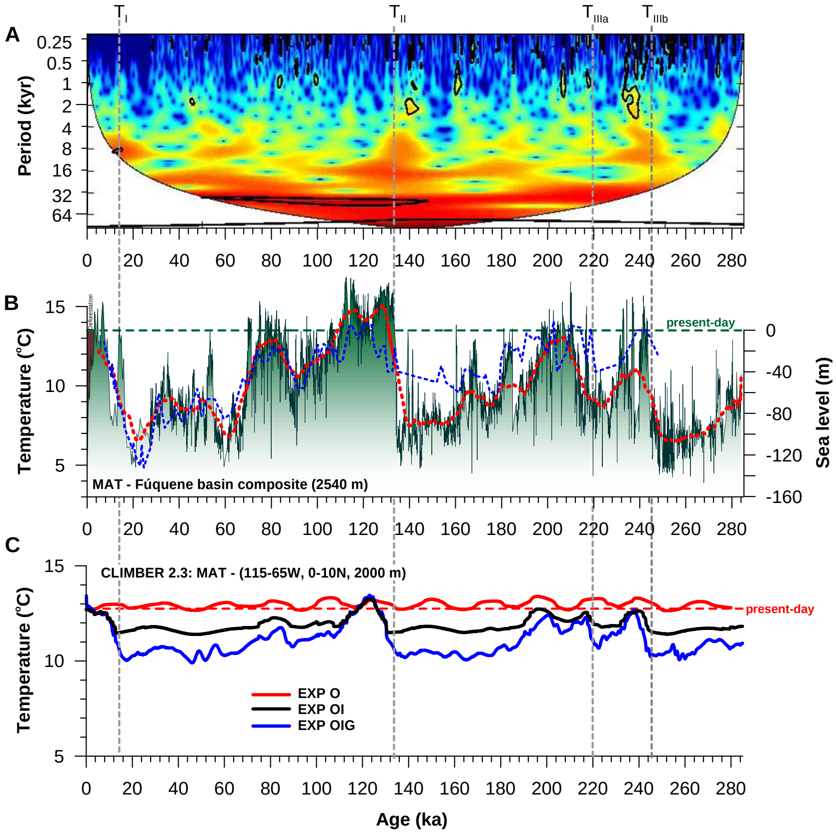


**Fig. 7.** Wavelet analysis of the Lake Fúquene arboreal pollen percentages (AP%) record **(A)** and comparison between the reconstructed **(B)** and modeled **(C)** mean annual temperatures (MAT) at Lake Fúquene. Red dotted line in (B) indicates 10 kyr moving average, while the blue dotted represents the radioisotopical dated coral-based sea level reconstructions (Thompson and Goldstein, 2006).





CPD
6, 2117–2158, 2010

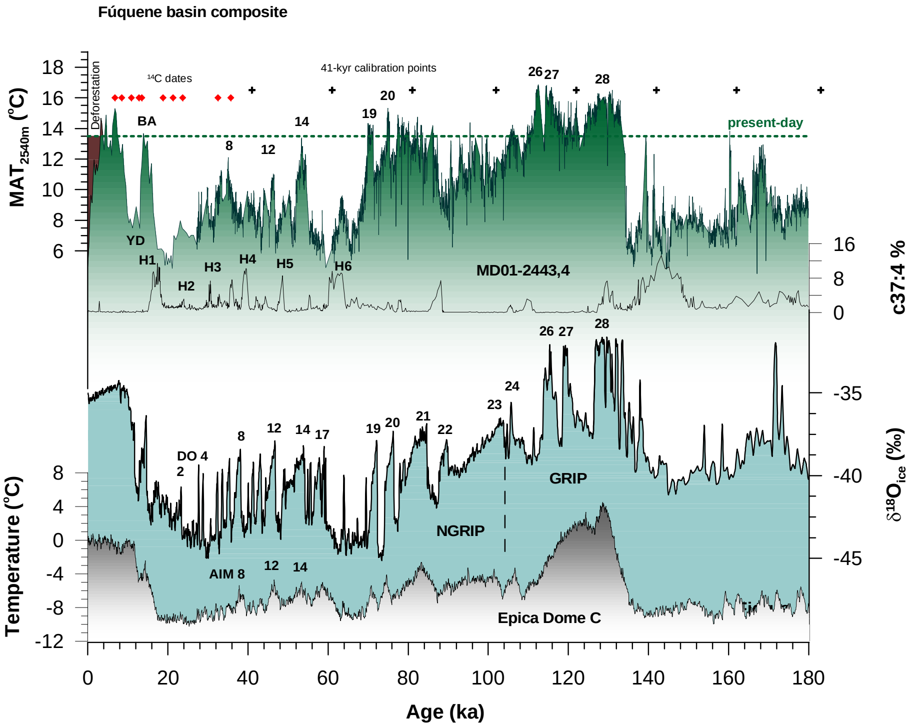


**Fig. 8.** Comparison between the reconstructed mean annual temperatures (MAT) at Lake Fúquene and the combined Greenland $\delta^{18}$O ice core records for the past 180 000 years (GRIP-Members, 1993) and temperature record of Epica Dome C (Jouzel et al., 2007; Parrenin et al., 2007). The DO numbers indicate Dansgaard-Oeschger cycles and AIM are the Antarctic Isotope Maxima (AIM). H1-H6 corresponds to the Heinrich events. BA = Bølling-Allerød interstadial and YD = Younger Dryas. The combined Greenland $\delta^{18}$O record includes (1) the Greenland Ice Core Chronology 2005 (GICC05) (NGRIP Members, 2004) based on annual layer counting for the past 60 ka, (2) the original NGRIP data (NGRIP Members, 2004; Svensson et al., 2008) between 60 and 103 ka, and (3) the data of GRIP below 103 ka.





CPD
6, 2117–2158, 2010